Campo, R. del, …et al. (2014). Mechanical properties and corrosion behavior of Mg–HAP composites. *Journal of the Mechanical Behavior of Biomedical Materials*, v. 39, pp.: 238-246.

DOI: https://doi.org/10.1016/j.jmbbm.2014.07.014

www.elsevier.com/locate/jmbbm

Mechanical properties and corrosion behavior of Mg-HAP composites

R. del Campo, B. Savoini, A. Muñoz, M.A. Monge, G. Garcés

PII: S1751-6161(14)00207-0
DOI: http://dx.doi.org/10.1016/j.jmbbm.2014.07.014
Reference: JMBBM1206

To appear in: *Journal of the Mechanical Behavior of Biomedical Materials*

Received date: 10 March 2014
Revised date: 2 July 2014
Accepted date:
15 July 2014

Cite this article as: R. del Campo, B. Savoini, A. Muñoz, M.A. Monge, G. Garcés, Mechanical properties and corrosion behavior of Mg-HAP composites, *Journal of the Mechanical Behavior of Biomedical Materials*, http://dx.doi.org/10.1016/j.jmbbm.2014.07.014

Mechanical properties and corrosion behavior of Mg-HAP composites

R. del Campo[1], B. Savoini[1], A. Muñoz[1], M.A. Monge[1] and G. Garcés[2]

[1] *Universidad Carlos III de Madrid, Departamento de Física, Avda. de la Universidad 30, 28911-Leganés, Madrid, Spain*

[2] *CENIM-CSIC, Departamento de Metalurgia Física, Avda. Gregorio del Amo 8, 28010-Madrid, Spain*

Corresponding author: begona.savoini@uc3m.es

Abstract

Mg and Mg-HAP composites containing 5, 10 and 15 wt.% of hydroxyapatite have been produced following a powder metallurgy route that consists of mixing raw powders and consolidation by extrusion. The microstructure, texture, mechanical behavior and resistance to corrosion under a PBS solution have been studied. Addition of HAP increases the microhardness of the composites, however the yield strength under compression slightly decreases. Texture analyses reveal a fiber texture for pure Mg that is weakened increasing the HAP fraction. This texture promotes twinning and softening of Mg and Mg-5HAP during the initial deformation stages. Mg-10HAP and Mg-15HAP present a strain-hardening dependence showing no softening. The volume fraction of HAP particles weakens the texture and favors the activation of secondary slip systems. Corrosion experiments in PBS solution have shown that Mg-5HAP exhibits the best resistance to corrosion. Texture and porosity appear to be the main material features controlling the corrosion rates of Mg-HAP composites under the present conditions.

1. Introduction

In the last years, magnesium-based compounds are attracting a great interest in different industrial sectors due to their possible technological applications. Magnesium-based materials are very attractive in the automobile and aerospace industries due to the low magnesium density and its high specific strength and stiffness (Hassan and Gupat, 2002). The low strength, low Young modulus and limited

room temperature ductility of pure magnesium could restrict the wide applicability of this material (de Garmo, 1979)]. However, the development of reinforced magnesium matrix composites or the addition of alloying elements, such as Al, Zr and rare earths seems to solve some of the difficulties related to the low ductility and low mechanical resistance of magnesium materials (Garcés et al. 2007; Qiuming et al. 2009 and Tang et al. 2011).

Magnesium is also a biocompatible and biodegradable element. Therefore magnesium-based materials are very striking for biomedical applications (Staiger et al. 2006 and Xue-Nan Gu et al. 2010). During decades, three types of metallic materials have been used for surgical implants, austenitic stainless steel, Co-Cr alloys and pure Ti and its alloys. The degradation of these metallic materials leads to toxic products that can cause long term complications, so, once the tissues have healed, it is necessary a second surgical procedure (Barrere et al. 2008; Best et al. 2008; Kannan et al. 2003; Niinomi, 2002 and Rack and Qazi, 2006). In recent years, due to the magnesium biodegradability and because it exhibits mechanical properties similar to natural bones, many investigations are being performed on magnesium materials so that they can be used in implants and prosthesis (Asit et al. 2010; Pietak et al. 2008 and Xingu et al. 2010). Its degradation produces the Mg^{2+} ions, which are already present in the human body, so it is expected to be non-toxic. The restriction in the implementation of magnesium as an orthopedic material is that the corrosion rate of Mg is too high and degradation starts before a stable tissue appears around the implant (Staiger et al. 2006). It is known that certain alloying elements as Ni, Al, Zr, Y or Nd improve the resistance of magnesium to corrosion (Kaesel et al. 2006; Shaw, 2003 and Song and Atrens, 2003). However some of them, as Al, Ni or Zr are toxic for the human body (Chashschin et al. 1994 and Thompson and Puleo, 1996). Another important point for a biomaterial is the ability of the implant to establish bonding with the surrounding bone tissue, i.e. the bioactivity of the implant. Therefore, it seems necessary to increase the bioactivity of magnesium-based materials. Introducing bioactive particles, as hydroxyapatite ($Ca_{10}(PO_4)_6(OH)_2$), that present a good ability to induce the deposition of Ca-P compounds can increase the surface biocompatibility and bioactivity of the matrix materials (Abdal-hay A. et al. 2013, Cao and Henc, 1996 and Chu et al. 2006).

In the present research work, different composites of magnesium-hydroxyapatite (Mg-HAP) have been produced following a powder metallurgy route that includes extrusion for consolidation. The microstructure of the composites has been characterized by X-Ray diffraction, optical microscopy and scanning electron microscopy. Mechanical properties have been studied by compression tests and microhardness measurements. Corrosion behavior under physiological pH conditions using phosphate buffered saline (PBS) solution has also been investigated.

2. Experimental Procedure

Mg-HAP composites with 5, 10 and 15 wt% of hydroxyapatite (2.9, 5.9 and 9.0 vol.%) were fabricated through a powder metallurgy route consisting of mixing the raw powders and consolidation by extrusion. The starting powders were magnesium with a purity of 99.8 % and a particle size <45 μm (Alfa Aesar) and hydroxyapatite (BABI-HAP-P) with a particle size <150 μm supplied by Berkeley Advanced Biomaterials. The raw powders were mixed in a Turbula Wab during 6 h, compacted in silicone moulds by cold isostatic pressing under a 250 MPa pressure and extruded in air at 673 K with a section reduction of 11 and a 2 mm/s speed. Bars with a 10 mm diameter were obtained. For comparison a bar of pure magnesium was also produced. The density of the sintered specimens was determined using a Helium Ultrapycnometer. The different phases present in the samples were investigated from X-Ray diffraction (XRD) measurements.

The microstructure of the extruded samples was analyzed by optical and scanning electron microscopy (SEM), and energy dispersion spectroscopy (EDS). The sample preparation consisted of grinding on SiC abrasive papers with different grit size and polishing with α-Al_2O_3 (0.3 μm particle size). In order to reveal the grains, etching was carried out in a solution of 1.5 g of picric acid, 25 ml of ethanol, 5 ml acetic acid and 10 ml of distilled water.

Texture analysis was performed by the Schulz reflection method, using a Siemens TM Kristalloflex D5000 diffractometer equipped with an Eulerian cradle. The X-radiation used was β-filtered Cu-K_α. The orientation distribution functions (ODFs) were computed from the measurement of (0002), $\left(10\bar{1}0\right)$, $\left(10\bar{1}2\right)$, $\left(10\bar{1}3\right)$ and $\left(11\bar{2}0\right)$ pole figures by the series expansion method. The reference system was selected with the Z-axis parallel to the extrusion direction.

The Vickers microhardness was measured at room temperature along longitudinal and transverse sections using an applied load of 9.81 N for 20 s. As microhardness value, the mean value of ten indentations, at least, was taken. The mechanical properties of the composites were studied from compressive tests carried out at room temperature on a universal tensile machine. Cylindrical specimens were machined along the extrusion direction with 6 mm diameter and 10.5 mm length. The compressive tests were done at a constant cross-head speed and a strain rate of 10^{-4} s. BN was used as lubricant in order to inhibit barreling. For each composition, at least three samples were tested to assure reproducibility.

Corrosion behavior of the samples was investigated under physiological pH conditions using a PBS (phosphate buffered saline, Sigma Aldrich) solution with the following concentration: 137 mM NaCl, 2.7 mM KCl and 10 mM phosphates. The corrosion rate was evaluated by collecting the hydrogen released from the reaction of Mg with PBS solution as it is described in previous studies (Zhiming and Andrej, 2011). Cylindrical samples were pasted at the bottom of a 1000 ml beaker containing 800 ml PBS solution. The sample surface exposed to the corrosion environment was ≈160 mm^2. All the experiments were performed at 37 ^oC. The hydrogen gas was collected by a filter funnel into a burette above the corroding sample. During the measurements, a test sample, immersed in an identical solution and at the same temperature was used to measure changes in the pH. The pH measurements were performed using a HI 3222 Hanna pHmeter.

3. Results and Discussion

3.1. Characterization of the extruded samples

The density measurements of the extruded samples are shown in Table I. The theoretical density value of the composites has been calculated from the mixing rule, considering that the theoretical density values of pure Mg and HAP are 1.738 and 3.11 g/cm^3, respectively. The densification of all materials is found to be in the range 94-96 %. For the Mg-HAP composites, a decrease of the densification with the HAP content is found.

Figs. 1b-d) show optical microscopy images of longitudinal sections of Mg and Mg-HAP extruded materials. The microstructure of the Mg sample consists of large grains elongated along the extrusion direction and grains much smaller with a large range of sizes and shapes. It is observed that on increasing the HAP content, the grain size diminishes and the grains tend to be equiaxed. Fig. 2 shows a BSE-SEM image of a Mg-15HAP sample. EDS analyses indicate that HAP (white contrast) is found homogeneously distributed within the magnesium matrix forming agglomerates. MgO particles (dark contrast) are also observed. These MgO particles are developed from the oxide layer formed in the surface of the Mg powder during the extrusion process. HAP volume fractions were computed from optical and SEM images, resulting in 2.3±0.2, 6.2±0.5 and 8.7±0.8 vol.% HAP values for 5, 10 and 15 wt.% HAP, respectively, in good agreement with the nominal ones. The phases present in the samples were determined by X-Ray diffraction using the CuK_α wavelength. The XRD patterns for the mixed Mg-15HAP and longitudinal sections of consolidated Mg-15HAP and pure Mg are compared in Fig 3. For the mixed powder (Fig. 3a), besides the Bragg reflections coming from Mg, some small peaks associated to HAP are also observed. For the consolidated samples (Fig. 3b and c) a Bragg peak due to MgO is also observed. This

confirms that the MgO particles are formed during the extrusion process. The diffraction pattern of the Mg-15HAP powder indicates a random orientation of the grains. However, the diffraction pattern of the Mg-15HAP consolidated material evidences a preferred orientation of the Mg grains with their basal planes, (0002), preferentially orientated parallel to the extrusion direction.

XRD patterns of consolidated Mg-5HAP and Mg-10HAP are similar to that found for Mg-15HAP, although the relative intensities from the HAP phase change with the content of HAP present in the sample. The ratio of the intensity for the (0002), reflection to the $\left(10\bar{1}0\right)$ one for pure Mg, 5, 10 and 15% HAP samples resulted in ≈17, ≈16, 12 and 8, respectively. The decrease of this value with the HAP content indicates a diminution of the fraction of grains orientated with their basal plane parallel to the extrusion direction.

Texture analyses were accomplished to determine the effect of the HAP content in the grain orientation. Fig. 4a-b) show the (0002)) and $\left(10\bar{1}0\right)$ pole figures of a transversal section for a pure Mg sample. These results agree with the characteristic fiber texture of extruded magnesium with basal planes parallel to the extrusion direction (Pérez et al. 2007). Fig. 4c) shows the intensity of the $\left(10\bar{1}0\right)$ pole figure as a function of the polar angle for Mg and the Mg-HAP materials. The texture intensity is higher for the Mg sample and decreases increasing the volume fraction of HAP. This texture reduction is due to the presence of the reinforcing particles, which stimulate the recrystallization of randomly-oriented grains in the adjacent regions of the particles by the particle stimulated nucleation mechanism, and modify the plastic flow of the magnesium particles changing their orientation (Garcés et al. 2005).

3.2. Mechanical properties

The Vickers microhardness of the different composites performed along the longitudinal and transverse sections are shown in Table II. The indentation sizes were in the range of ≈140 μm, four or five times larger than the mean value of HAP particles (see Fig. 2). According to the measurements, the microhardness increases on adding HAP particles and, furthermore, increasing the HAP content. The microhardness values for the transversal section are significantly higher than the corresponding for the longitudinal planes. This behavior is related to the lower mean grain size in the transverse section. Furthermore, the difference between these microhardness values decreases on increasing the HAP content (Table II). This tendency was also observed on reinforcing Mg with Y_2O_3 particles (Garcés et al. 2006 and Huajie et al. 2008). As was previously demonstrated, the reinforcement particles tend to prevent the appearance

of the texture induced by the extrusion process and therefore to eliminate the microhardness anisotropy induced by the texture.

The compressive curves of pure Mg and Mg-HAP composites are presented in Fig. 5. The most characteristic parameters of the compressive curves are shown in Table III. The yield strength of pure Mg is slightly higher than that of Mg-HAP and slightly tends to decrease on increasing the HAP content. The yield strength is defined as the applied stress at 0.2 % of plastic deformation. In Mg at room temperature, the critical resolved shear stress (CRSS) for the basal slip system is much lower than those of the non-basal slip systems on prismatic and pyramidal planes. Extruded Mg exhibits a strong $\left(10\bar{1}0\right)$ fiber texture, therefore, in case the material is deformed along the extrusion direction the basal slip system is blocked in most of the grains. However, a slight misalignment of the basal plane can lead to the operation of this slip mode. According to the results shown in Fig. 4), the intensity of texture decreases on increasing the HAP content, which implies that more grains have favorable orientations for basal slip. This would result in lower values of the yield strength.

Another remarkably feature in the compression curve of non-reinforced magnesium is a yield diminution once the yield strength is reached and the subsequent gradual increase of the hardening until fracture. It is well known that twinning deformation plays an important role during the deformation of magnesium at room temperature (Agnew et al. 2001 and Wang Y.N. and Huang J.C., 2007). During compression, $\left\{10\bar{1}2\right\}10\bar{1}0$ twinning is activated in those grains having their c-axis oriented perpendicular to the compression axis. Due to the $\left(10\bar{1}0\right)$ texture developed in the extruded Mg, after the yield strength is reached, the matrix deforms by twinning in the $\left\{10\bar{1}2\right\}10\bar{1}0$ system and the stress decreases. This is confirmed by the microstructure of the longitudinal section of a compressed Mg sample deformed to failure, as shown in Fig. 6, where a large number of deformation twins are found. Once the twinning process is exhausted, the strain-hardening rate increases rapidly. This increase is due to a) the new barriers to dislocation movements introduced by the twinning process, b) the reorientation of the Mg grains and slip-twinning interaction and c) the lower motion of the dislocations inside the twinned grains (Agnew et al. 2001 and Karaman, 2000). The hardening onset in Mg-5HAP compression curves appears at somewhat lower strains than in the curves for pure Mg. In contrast, Mg-10HAP and Mg-15HAP exhibit compression curves without evidences of softening attributable to twinning. This behavior is consistent with the decrease of the fiber texture with the HAP content. As the volume fraction of HAP particles increases, the intensity of the texture

diminishes, different slip systems to the basal one may be active, and twinning does not occur.

3.3 Corrosion behavior

The study of the corrosion of pure magnesium and Mg-HAP composites was carried out following the method described by Zhiming and Atrens (Zhiming and Andrej, 2011). In this configuration, the Mg corrosion is evaluated from measuring the H_2 volume released in the solution. The corrosion experiments were done by immersing the samples in PBS solution during 100 hours. The H_2 released during the experiment was gathered in a burette and its volume was measured versus time. For each composition 3 samples were used. The Mg corrosion in aqueous environment is given by the following overall reaction (Zhiming and Andrej, 2011):

$$Mg + 2H_2O \rightarrow Mg(OH)_2 + H_2 \quad (1)$$

According to this overall reaction, one molecule of hydrogen is evolved for each atom of corroded Mg. On taking into account this data, it is possible to determine the magnesium mass loss rate from the volume rate of H_2 released during the corrosion experiment. The procedure followed for evaluating the magnesium mass loss rate is described in detail in ref. (Zhiming and Andrej, 2011).

Fig. 7 shows the evolution of the solution pH with the immersion time for Mg and Mg-HAP composites. The magnesium corrosion as a result of the H^+ reduction in presence of Mg is related with the H_2 production by Eq. 1. Thus, the formation of H_2 causes the rise of the pH value of the medium. Since PBS is a buffer solution with capability to regulate the pH variations, a high rate of pH increase indicates that strong magnesium corrosion occurs. From Fig. 7 it is inferred that addition of 5 wt% HAP slightly reduces the corrosion rate with respect to pure Mg.

Fig. 8 presents the volume of H_2, V_H, released during the experiment normalized to the initial area of the sample for all materials. The increase in the corrosion rate was accompanied by a substantial change in the pH value (see Fig. 7). The H_2 volume rate was converted to an average corrosion penetration rate, given in mm/year (Zhiming and Andrej, 2011). The results are shown in Fig. 9. According to these results, Mg-5HAP exhibits the best resistance to corrosion and Mg-15HAP the worst. There are many parameters that have an effect on the corrosion of the Mg-HAP composites. The most important parameters are related with the microstructure of the composites, such as texture, grain size and porosity. The presence of HAP can also affect to the magnesium corrosion, although HAP in PBS exhibits a high resistance to corrosion. In fact, HAP is used as a coating material in magnesium alloys to improve their resistance to corrosion (Song et al. 2008; Wen et al. 2009; Yang et al. 2008 and Zhang et al. 2010). The

resistance to corrosion of HAP is obvious in Fig. 10. X-ray diffraction pattern of the corrosion products shown in Fig. 11 reveals that they primarily consist of $Mg(OH)_2$ powder with a small fraction of HAP. On the other hand, the influence of the grain size on the corrosion rate in Mg and Mg alloys is not clear, as controversial results have been found (Argade et al. 2012; Dan Song et al. al 2010 and Naing and Wei, 2010). It is accepted that the corrosion resistance depends on the grain size, via the grain boundary defects. In the surface of the Mg alloys a protective passive film of $Mg(OH)_2$ is formed. The appearance and growth of this protective layer is facilitated by the existence of nucleation sites associated with the defects present in the grain boundaries. Therefore, the smaller the grain size the faster the development of the protective $Mg(OH)_2$ layer. The growth of $Mg(OH)_2$ is accomplished by OH^- diffusion from the PBS solution into the Mg matrix as Fig. 10 reveals. Meanwhile the integrity of this layer is retained during its growing it acts as a barrier for ions coming from the PBS solution and favors the corrosion resistance. Once the layer failure is initiated the cracks increases the OH^- diffusivity across the layer, and matrix corrosion becomes faster. The substantial amounts of hydrogen released would contribute to the destruction of the protective $Mg(OH)_2$ layer. The small differences in the grain sizes of the present Mg-HAP composites would not account for the differences observed in their corrosion rates.

The effect of texture and porosity in the corrosion rate would also be considered. It has been found in magnesium that (0001) surfaces exhibit a better corrosion resistance than $\left(10\bar{1}0\right)$ and $\left(10\bar{1}2\right)$ and surfaces. Surfaces with higher atomic density have lower surface energy, thus atoms on these surfaces are dissolved slower (Guang-Ling et al. 2010; Ming et al. 2008 and Renlong et al. 2011). As the pole figures show, a great number of (0001) planes, resistant to corrosion, are parallel to the surface of the samples of pure magnesium. On increasing the HAP content less (0001) planes are parallel to the surface, and lower the resistance to corrosion. Mg-15HAP is the composite with the weakest texture and, consequently, with the lowest resistance to corrosion. Porosity favors the magnesium corrosion and is higher in Mg-15HAP than in Mg-10HAP and Mg-5HAP. Then, texture and porosity should be the main material features controlling the corrosion rates of Mg-HAP composites.

4. Conclusions

Pure magnesium and Mg-HAP composites containing 5, 10 and 15 wt.% of hydroxyapatite have been produced by a powder metallurgy route and consolidation by extrusion. The relative density of the composites decreases increasing the HAP content from 96 % to 94%. The pure Mg exhibits a microstructure of large grains

elongated along the extruded direction and a strong fiber texture with the c-axis perpendicular to the extrusion direction. On increasing the HAP content the intensity of the texture decreases, the grains tend to be equiaxed and their size diminishes.

Addition of HAP increases the microhardness, however the yield strength under compression slightly decreases. Because of the fiber texture of pure Mg, deformation beyond the yield point is produced by $\left\{10\bar{1}2\right\}1\bar{0}10$ twinning, inducing softening, followed by strain-hardening after the twinning process is exhausted. Mg-5HAP exhibits similar behavior. Mg-10HAP and Mg-15HAP present a strain-hardening dependence showing no softening. The volume fraction of HAP particles weakens the texture and favors the activation of secondary slip systems.

Corrosion experiments in PBS solution have shown that Mg-5HAP exhibits the best resistance to corrosion. Texture and porosity appear to be the main material features controlling the corrosion rates of Mg-HAP composites under the present conditions.

Acknowledgments

This work has been supported by the Regional Government of Madrid through the ESTRUMAT-CM program (MAT-1585). R del Campo thanks to the Universidad Carlos III de Madrid for the support.

References

Abdal-hay A., Barakat N., Lim J. K., Ceram. Int. 39 (2013) 183-195, Hydroxyapatite-doped poly(lactic acid) porous film coating for enhanced bioactivity and corrosion behavior of AZ31 Mg alloy for orthopedic applications

Agnew S. R., Yoo M. H. and Tome C. N., Acta Mater. 49 (2001) 4277–4289, Application of texture simulation to understanding mechanical behavior of Mg and solid solution alloys containing Li or Y

Argade G.R., Panigrahi S.K., Mishra R.S., Corrosion Sci. 58 (2012) 145-151. Effects of grain size on the corrosion resistance of wrought magnesium alloys containing neodymium

Asit K.K., Hwa C.H., Seung H.Y., Kug S.H. and Kwang S.S., Bull. Mater. Sci. 33 (2010) 43-47. Microstructure and mechanical properties of Mg-HAP composites

Barrere F., Mahmood T. A., de Groot K., van Blitterswijk C.A., Mater. Sci. Eng. R-Rep. 59 (2008) 38-71. Advanced biomaterials for skeletal tissue regeneration: Instructive and smart functions

Best S.M., Porter A.E., Thian E.S., Huang J., J. Eur. Ceram. Soc., 28, (2008) 1319-1327. Bioceramics: Past, present and for the future

Cao W. P., Hench L. L., Ceram. Int. 22 (1996) 493. Bioactive materials

Chashschin V., Artunina P. and Norseth T., Sci. Total Env. 148 (1994) 287-291. Congenital defects, abortion and other health effects in nickel refinery workers

Chu C., Xue X., Zhu J., Yin Z., J. Mater. Sci.: Mater. Med. 17 (2006) 245-251. Fabrication and characterization of titanium-matrix composite with 20 vol% hydroxyapatite for use as heavy load-bearing hard tissue replacement

Dan Song A. M., Jinghua J., Pinghua L., Donghui Y., Junfeng F., Corrosion Sci. 52 (2010) 481-490. Corrosion behavior of equal-channel-angular-pressed pure magnesium in NaCl aqueous solution

De Garmo P.E. Materials and processes in manufacturing, 5th ed. New York: Collin Macmillan (1979)

Garcés G., Pérez P., Adeva P., Scr. Mater. 52 (2005) 615-619. Effect of the extrusion texture on the mechanical behaviour of Mg–SiCp composites

Garcés G., Rodríguez M., Pérez P., Adeva P., Mat. Sci. Eng A-Struct. 419 (2006) 357–364. Effect of volume fraction and particle size on the microstructure and plastic deformation of Mg–Y2O3 composites

Garcés G., Rodríguez M., Pérez P., Adeva P., Compos. Sci. Technol. 67 (2007) 632-637. High temperature mechanical properties of Mg–Y2O3 composite: Competition between texture and reinforcement contributions

Guang-Ling S., Mishra, R, ZhenQing X., Electrochem. Commun. 12 (2010) 1009–1012. Crystallographic orientation and electrochemical activity of AZ31 Mg alloy

Hassan S.F., Gupat M., Mater. Res. Bull. 37 (2002) 377–389. Development of a novel magnesium–copper based composite with improved mechanical properties

Huajie Y., Shuming Y., Chongxiang H., Zhefeng Z., Shiding W., Shuxin L. and Yandong L., Adv. Eng. Mater., 10 (2008) 955-960. EBSD study on deformation twinning in AZ31 magnesium alloy during quasi-in-situ compression

Jiang Q.C., Wang H.Y., Wang J.G., Guan Q.F., Xu C.L., Mater. Lett. 57 (2003) 2580–2583. Fabrication of TiCp/Mg composites by the thermal explosion synthesis reaction in molten magnesium

Kaesel V., Tai P.T., Bach Fr.W., Haferkamp H., Witte F. and Windhagen H. 6th International Conference Magnesium Alloys and Their Applications, (Wiley-Vch, 2006)

Kannan S., Balamurugan A., Rajeswari S., Mater. Lett. 57 (2003) 2382-2389. Hydroxyapatite coatings on sulfuric acid treated type 316L SS and its electrochemical behaviour in Ringer's solution

Karaman I., et al., Acta Mater. 48 (2000) 2031–2047. Modeling the deformation behavior of Hadfield steel single and polycrystals due to twinning and slip

Ming L., Dong Q., Ming-Chun Z., Guangling S. and Atrens A., Scr. Mater. 58 (2008) 421-424. The effect of crystallographic orientation on the active corrosion of pure magnesium.

Naing Naing A., Wei Z., Corrosion Sci. 52 (2010) 589-594. Effect of grain size and twins on corrosion behaviour of AZ31B magnesium alloy

Niinomi M., M. Metall Mater Trans A 33 (2002) 477-486. Recent metallic materials for biomedical applications

Pérez P., Garcés G., Adeva P., J. Mater. Sci. 42 (2007) 3969-3976. Influence of texture on the mechanical properties of commercially pure magnesium prepared by powder metallurgy

Pietak A., Mahoney P., Dias G.J., Staiger M., J. Mater. Sci: Mater. Med. 19 (2008) 407-415. Bone-like matrix formation on magnesium and magnesium alloys

Qiuming P., Xiuli H., Lidong W., Yaoming W., Zhanyi C., Limin. W., Mater. Des. 30 (2009) 292–296. Microstructure and mechanical properties of high performance Mg–Gd based alloys

Rack H.J., Qazi J.I., Mater. Sci. Eng. C 26 (2006) 1269-1277. Titanium alloys for biomedical applications

Renlong X., Bo L., Ling L., Qing L., Mater. Des. 32 (2011) 4548–4552. Influence of texture on corrosion rate of AZ31 Mg alloy in 3.5wt.% NaCl

Shaw B., Corrosion resistance of magnesium alloys. ‘‘ASM Handbook Volume 13 A: Corrosion: Fundamentals, Testing and Protection’’. D. Stephen (ASM Int., United Kingdom, 2003).

Shi Z, Atrens A, Corrosion Sci. 53 (2011) 226-246. An innovative specimen configuration for the study of Mg corrosion

Song G. and Atrens A., Adv. Eng. Mater. 5 (2003) 837. Understanding Magnesium corrosion

Song Y.W., Shan D.Y., Han E.H., Mater. Lett. 62 (2008) 3276–3279. Electrodeposition of hydroxyapatite coating on AZ91D magnesium alloy for biomaterial application

Staiger M.P., Pietak A.M., Huadmai J., Dias G., Biomaterials, 27 (2006) 1728-1734. Effect of the Zn content on the microstructure and mechanical properties of indirect-extruded Mg–5Sn–xZn alloys

Tang W. N., Park S.S., You B.S., Mater. Des. 32 (2011) 3537-3543. Effect of the Zn content on the microstructure and mechanical properties of indirect-extruded Mg–5Sn–xZn alloys

Thompson G. and Puleo D., Biomaterials 17 (1996) 1949. Ti-6Al-4V ion solution inhibition of osteogenic cell phenotype as a function of differentiation time course in vitro

Wang Y.N. and Huang J.C., Acta Mater. 55 (2007) 897-905. The role of twinning and untwining in yielding behavior in hot-extruded Mg-Al-Zn alloy

Wen C., Guan S., Peng L., Ren C., Wang X., Hu Z., Appl Surf Sci 255 (2009) 6433–6438. Characterization and degradation behavior of AZ31 alloy surface modified by bone-like hydroxyapatite for implant applications

Xingu Y., Minfang C., Meng Y., Jun W. and Debao L., J. Mater. Sci: Mater. Med. 21 (2010) 1321-1328. In vitro corrosion resistance and cytocompatibility of nano-hydroxyapatite reinforced Mg–Zn–Zr composites

Xue-Nan Gu, Yu-Feng Zheng, Front. Mater. Sci. China 4 (2010) 111-115. A review on magnesium alloys as biodegradable materials

Yang J.X., Jiao Y.P., Cui F.Z., Lee In-Seop, Yin Q.S., Zhang Y., Surf. Coat. Tech. 202 (22–23) (2008) 5733–5736. Modification of degradation behavior of magnesium alloy by IBAD coating of calcium phosphate

Zhang C.Y., Zeng R.C., Liu C.L., Gao J.C., Surf. Coat. Tech. 204 (2010) 3636–3640. Comparison of calcium phosphate coatings on Mg–Al and Mg–Ca alloys and their corrosion behavior in Hank's solution

TABLES

Table I. Theoretical and experimental density values for Mg and Mg-HAP composites.

Sample	ρ_{theo} (g/cm^3)	ρ_{exp} (g/cm^3)	ρ_{exp} /ρ_{theo} (%)
Pure Mg	1.738	1.630	93.8
Mg-5HAP	1.777	1.714	96.4
Mg-10HAP	1.818	1.746	96.0
Mg-15HAP	1.861	1.749	94.0

Table II. Vickers microhardness measured in the longitudinal, H_V(L), and transverse, H_V(T), sections.

Sample	H_V(L) (MPa)	H_V(T) (MPa)	(H_V(T)- H_V(L)) / H_V(L) %
Pure Mg	490±10	519±5	5.6
Mg-5HAP	530±10	560±10	5.4
Mg-10HAP	580±10	593±7	2.2
Mg-15HAP	610±10	623±9	2.1

Table III. Yield strength, ultimate compression strength and failure strain calculated from the compressive curves.

Sample	Yield strength (MPa)	Ultimate Compression strength (MPa)	Failure strain
Pure Mg	224	340	0.131
Mg-5HAP	222	452	0.185
Mg-10HAP	219	415	0.175
Mg-15HAP	216	371	0.223

Figure Captions

Fig. 1. Optical microscopy images of Mg and Mg-HAP composites. In Mg-HAP dark areas correspond to hydroxyapatite particles.

Fig. 2. BSE-SEM image of a Mg-15HAP sample showing HAP (white) and MgO (dark).

Fig. 3. X-Ray diffraction patterns of (a) Mg-15HAP powder, (b) consolidated Mg-15HAP and (c) consolidated Mg.

Fig. 4. Pole figures of (a) (0002) and (b) $\left(10\bar{1}0\right)$ planes of Mg and (c) pole figure intensity of $\left(10\bar{1}0\right)$ plane as a function of the polar angle for consolidated Mg (■), Mg-5HAP(★), Mg-10HAP(▲) and Mg-15HAP(●).

Fig. 5. Compressive curves of Mg and Mg-HAP composites measured at room temperature.

Fig. 6. Microstructure from the longitudinal section of a Mg sample deformed under compression to failure, showing intense twinning.

Fig. 7. Evolution of the solution pH with the immersion time for Mg and Mg-HAP.

Fig. 8. Hydrogen released volume normalized to initial area with the immersion time for Mg and Mg-HAP.

Fig. 9. Evolution of the corrosion penetration rate for samples immersed 100 h in PBS solution.

Fig. 10. Cross-section BSE-SEM images of the corroded layer formed on Mg and Mg-15HAP after a 100 h immersion in PBS.

Fig. 11. X-Ray diffraction pattern of the corrosion products layer detached from Mg-15HAP.

- Pure Mg and Mg-xHAP (x=5, 10, 15 wt.%) composites have been produced by extrusion
- Mg develops a fiber texture that is weakened increasing the HAP fraction
- Texture promotes twinning of Mg and Mg-5HAP during the initial deformation stages
- Mg-5HAP exhibits better resistance to corrosion in PBS solution than Mg

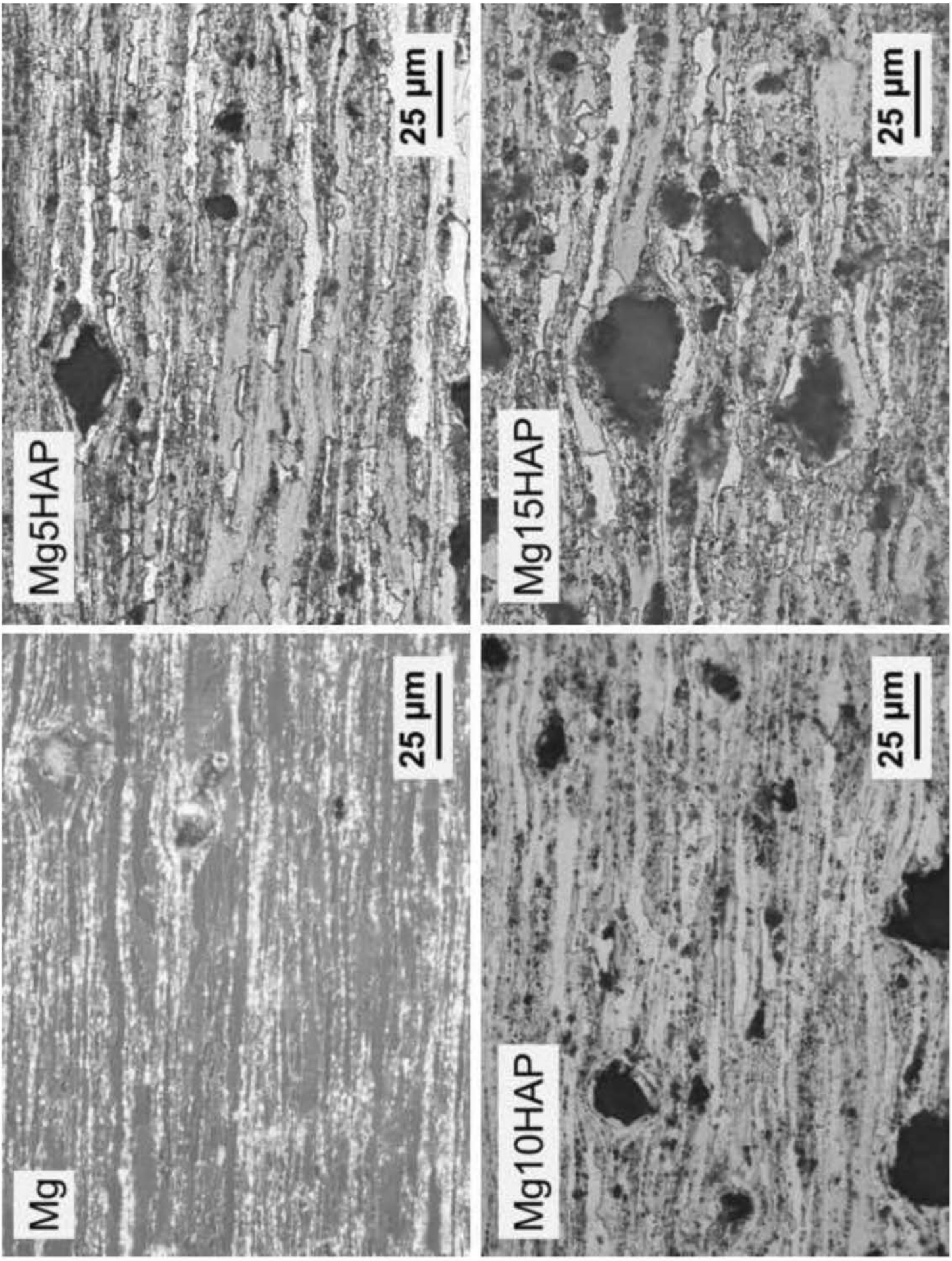

Figure

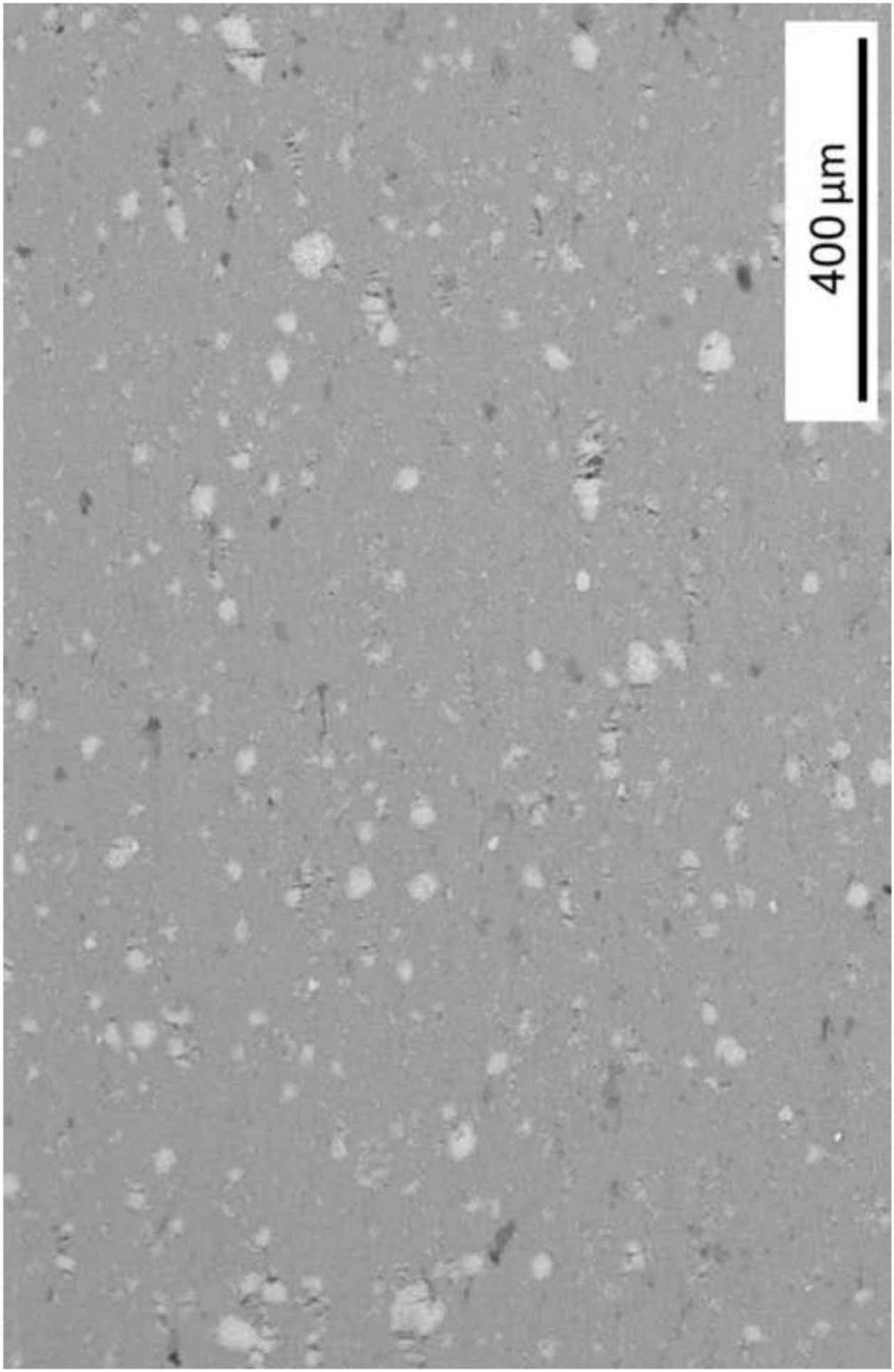

Figure2

Figure3

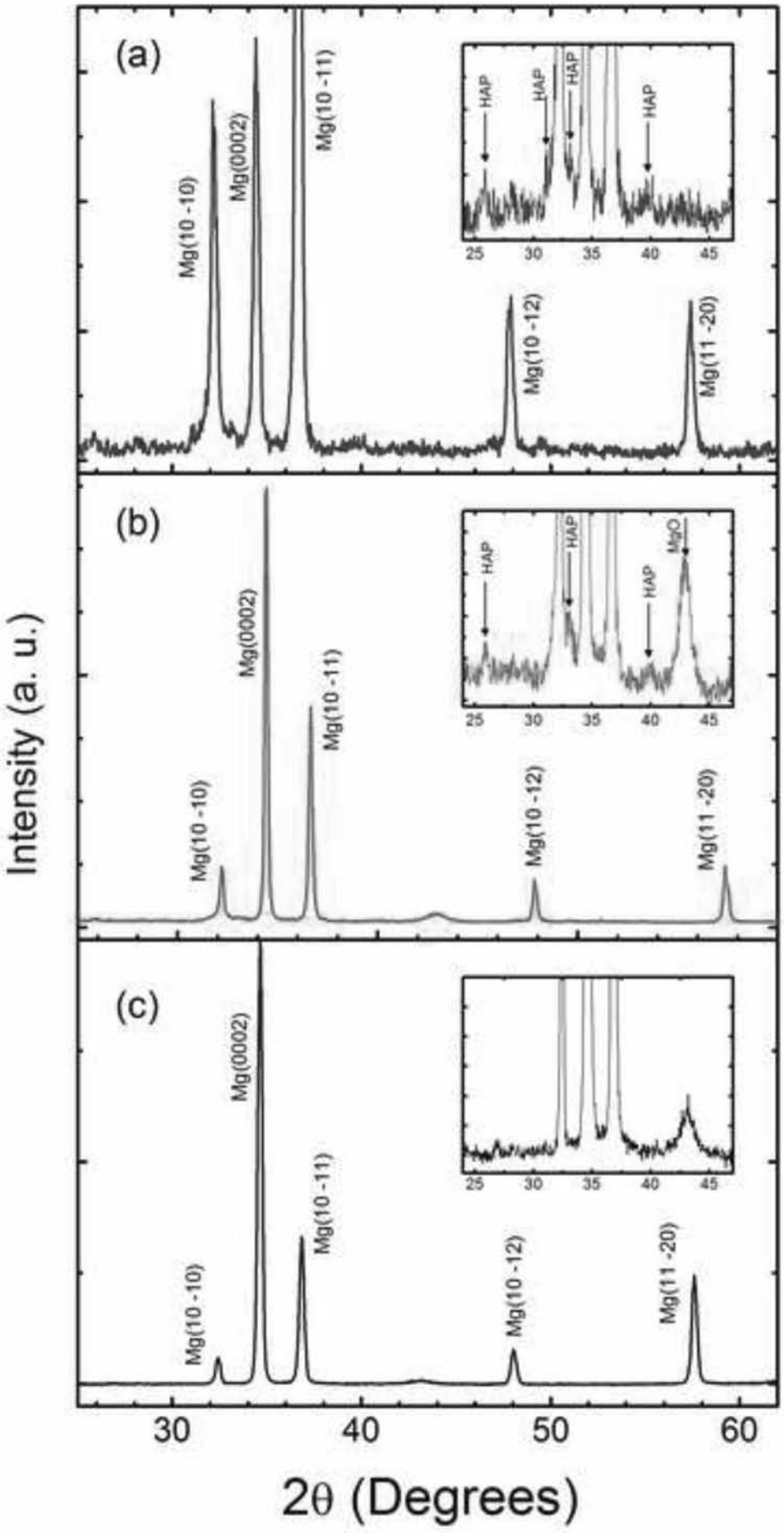

Figure4

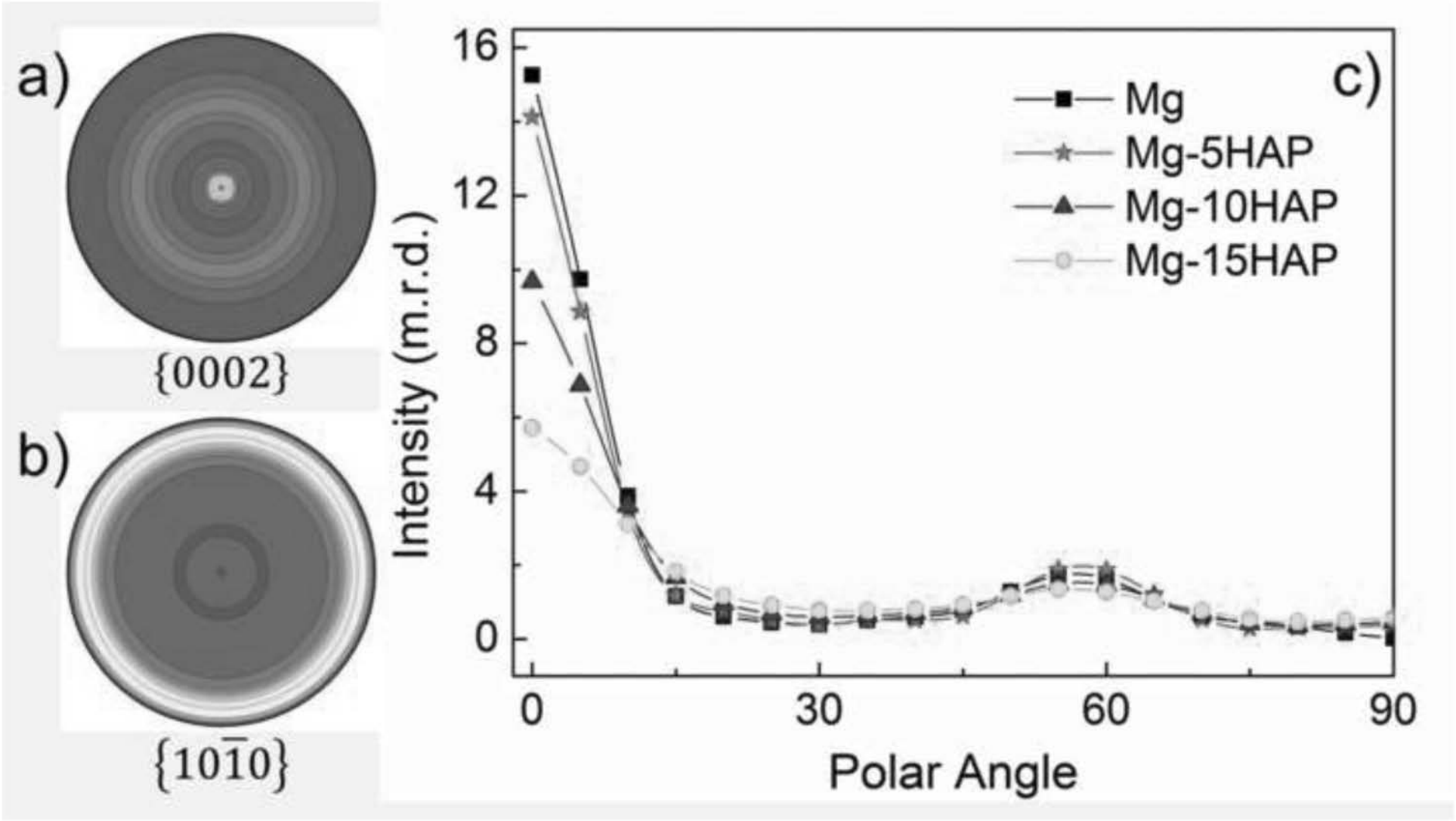

Figure5

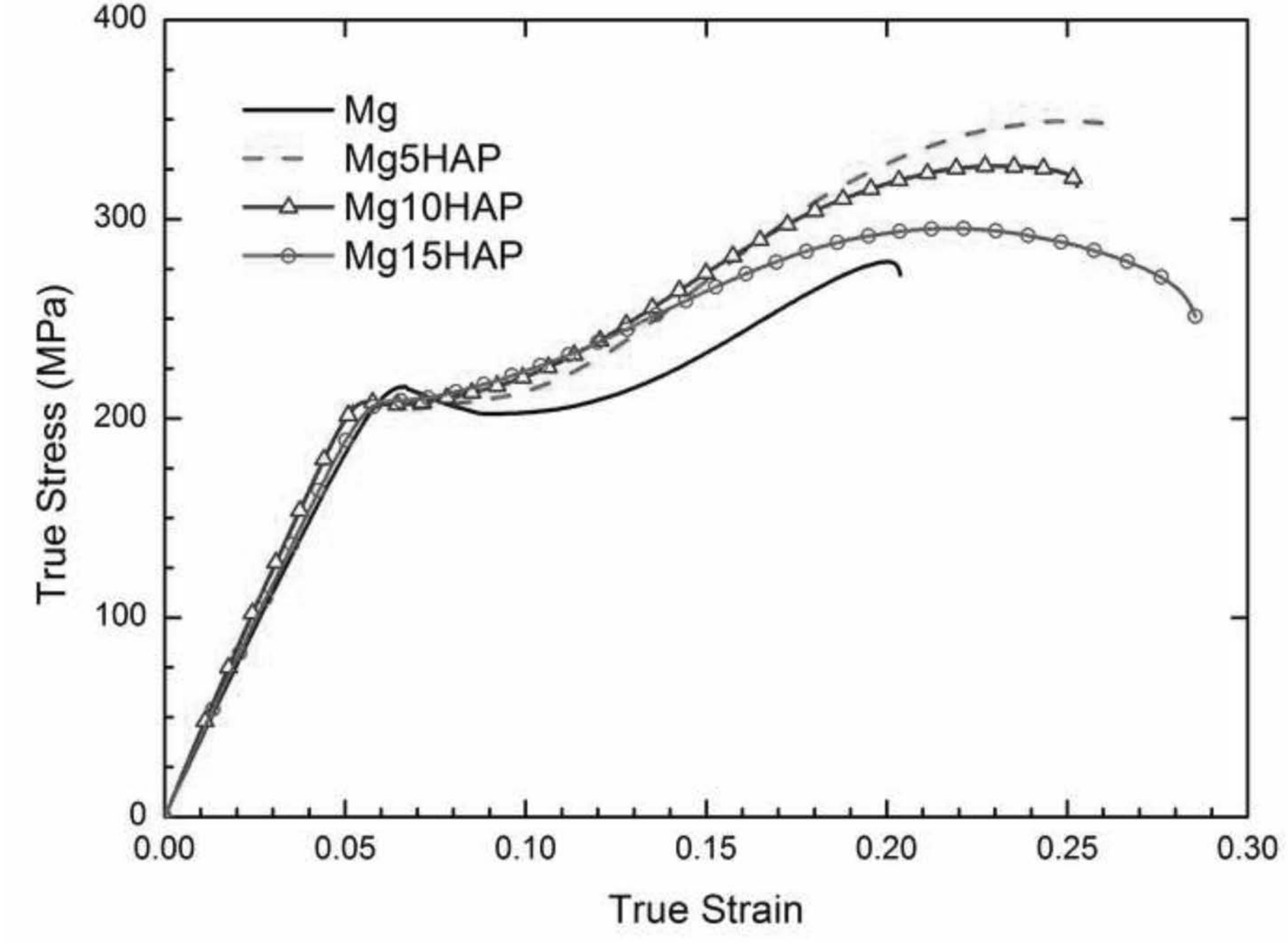

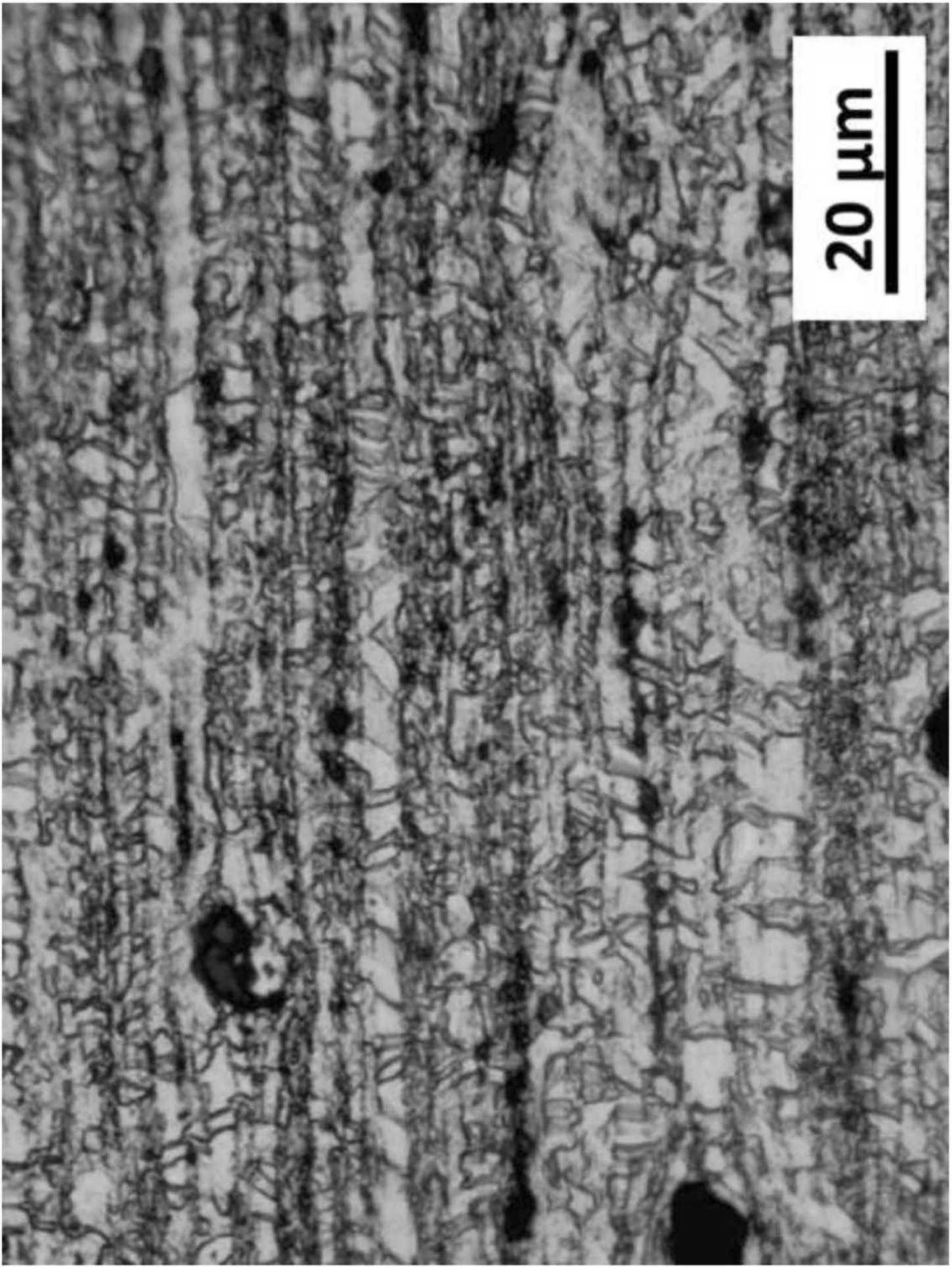

Figure6

Figure7

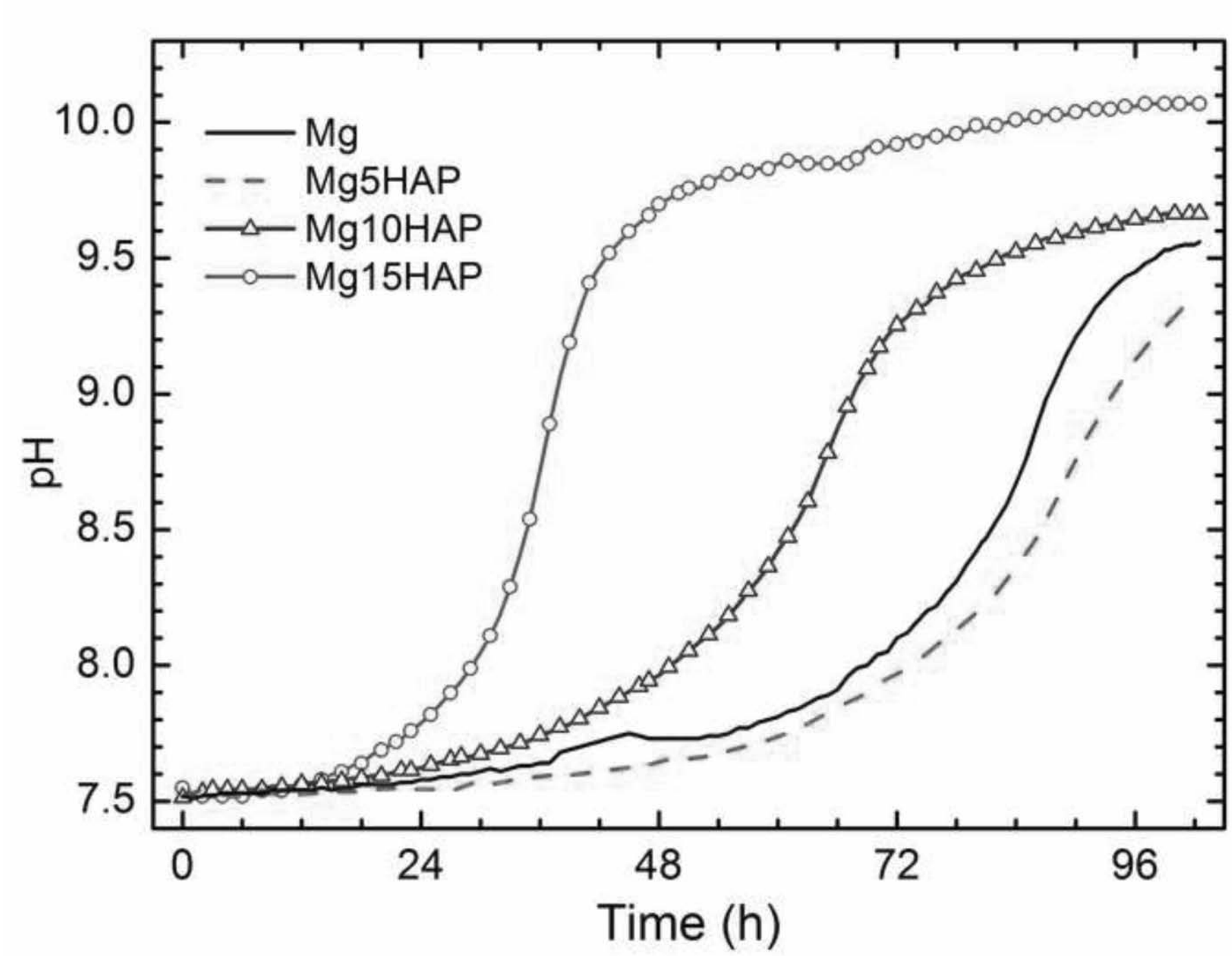

Figure8

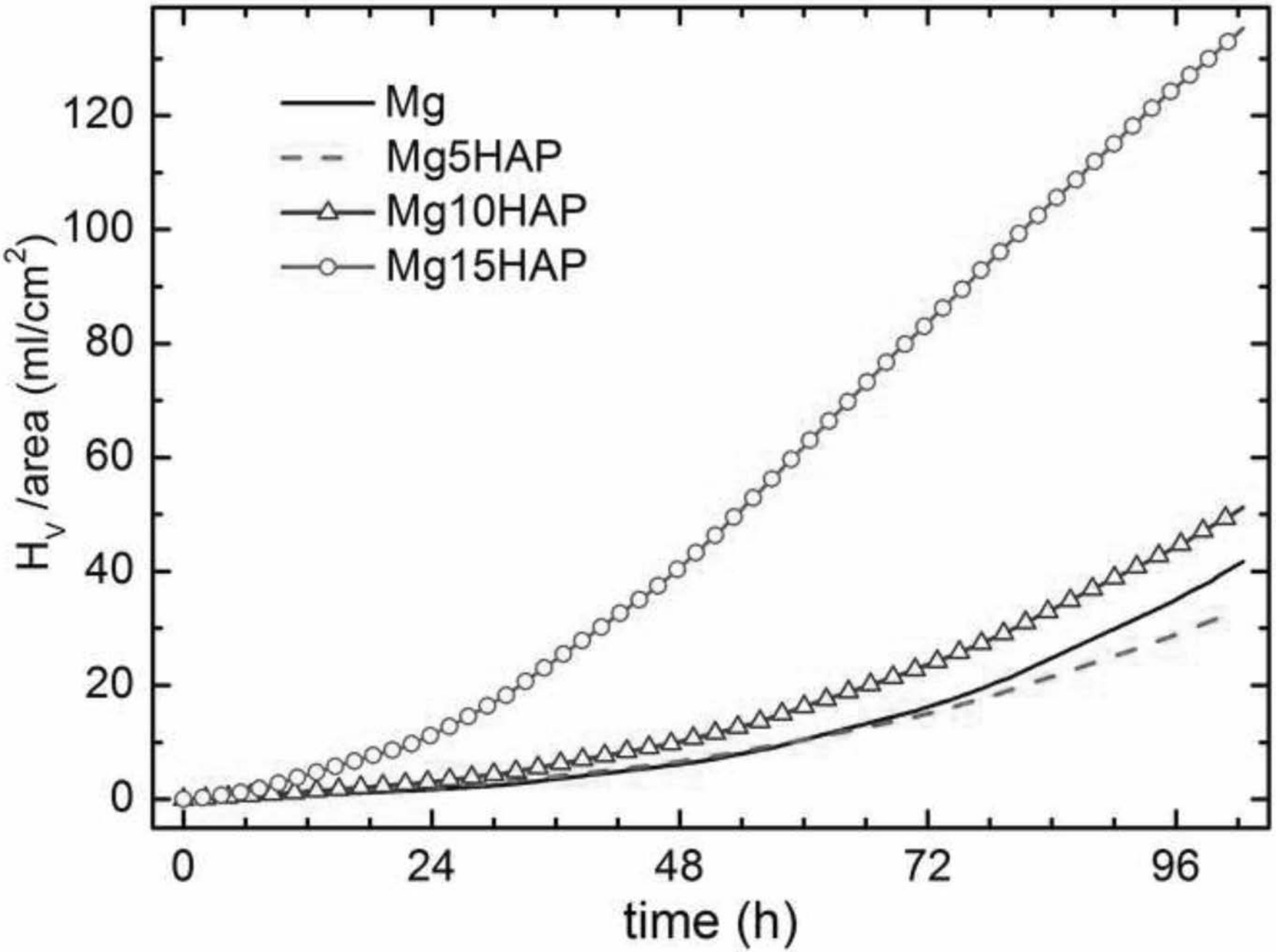

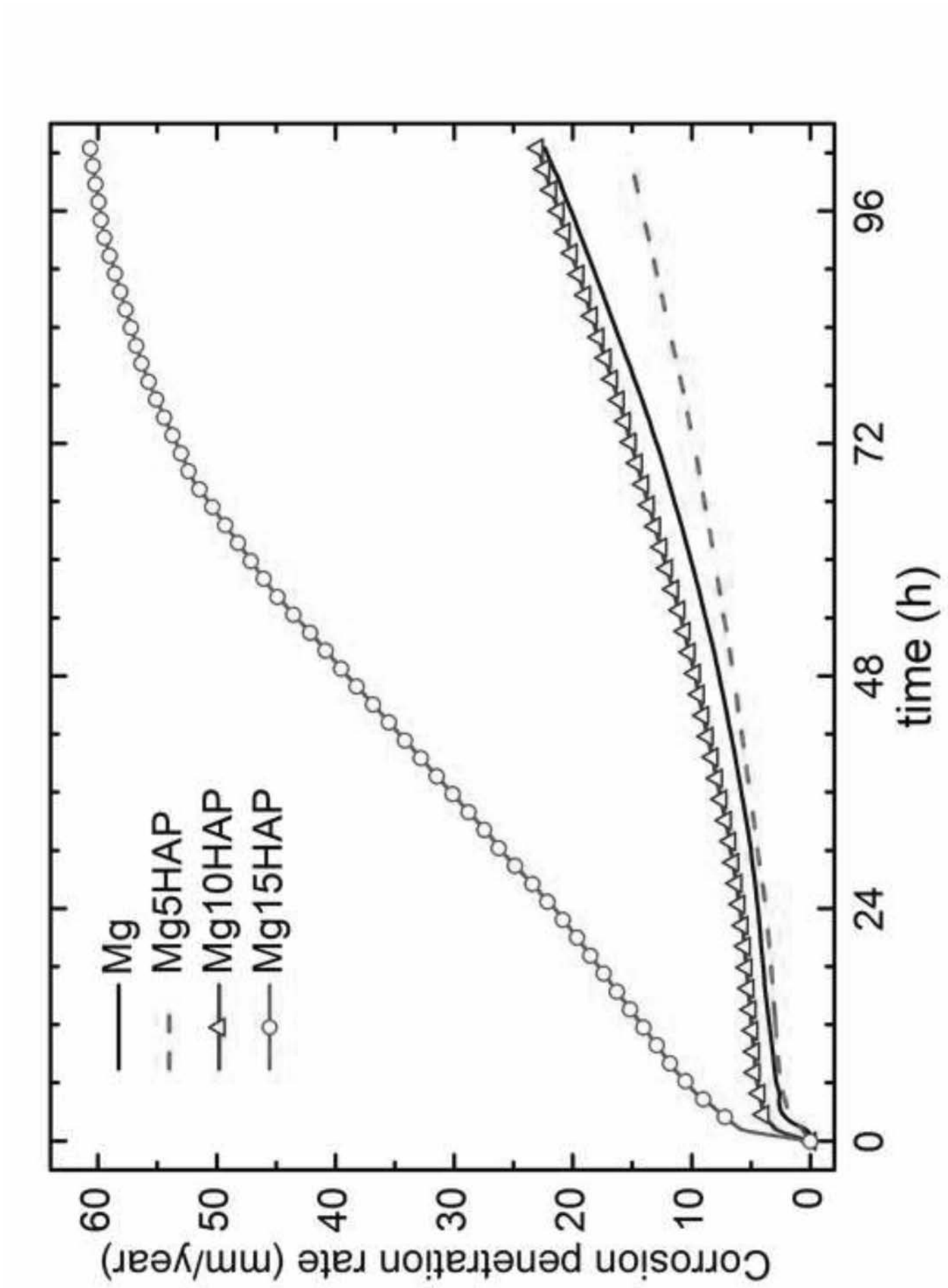

Figure9

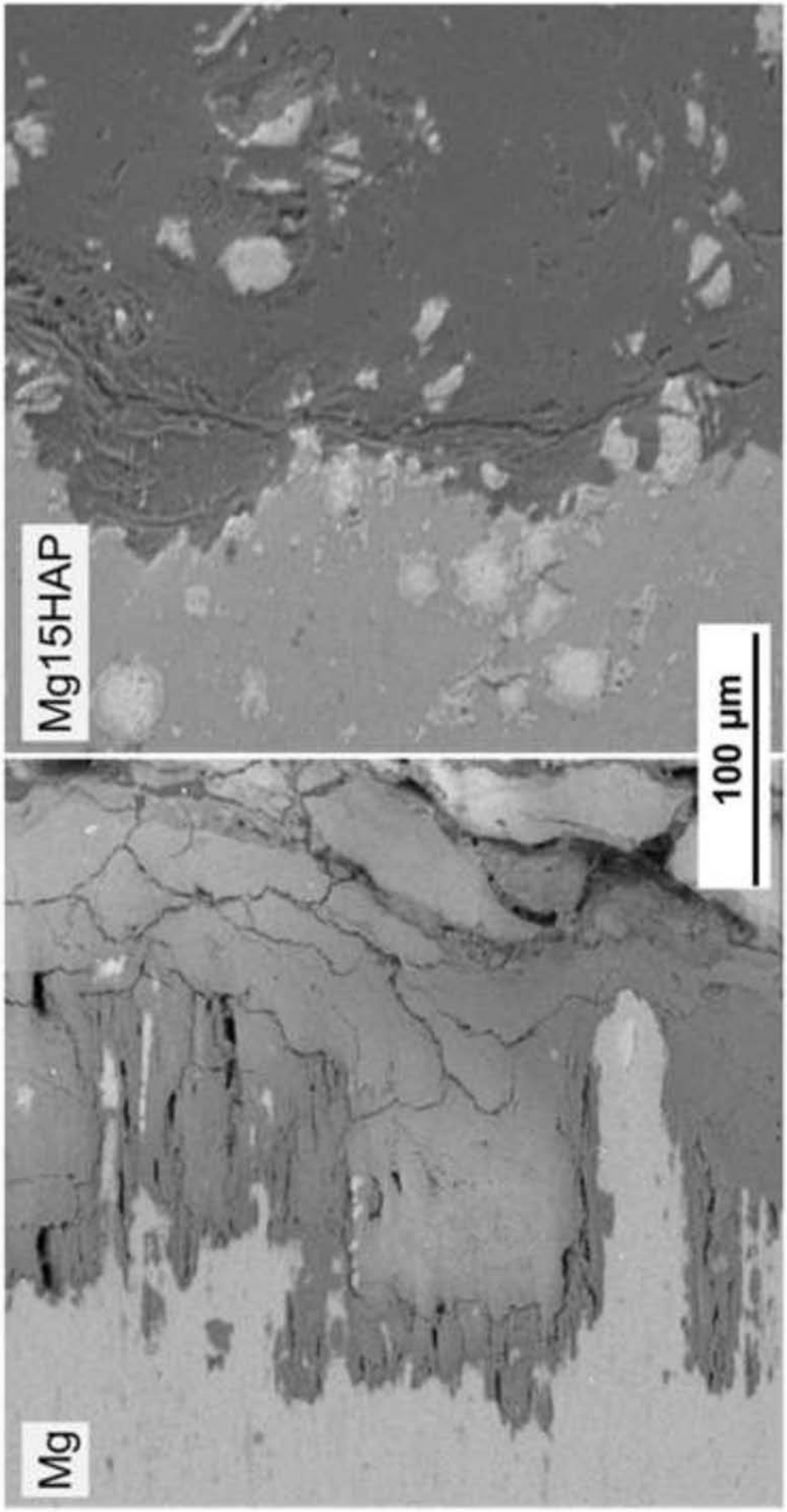

Figure10

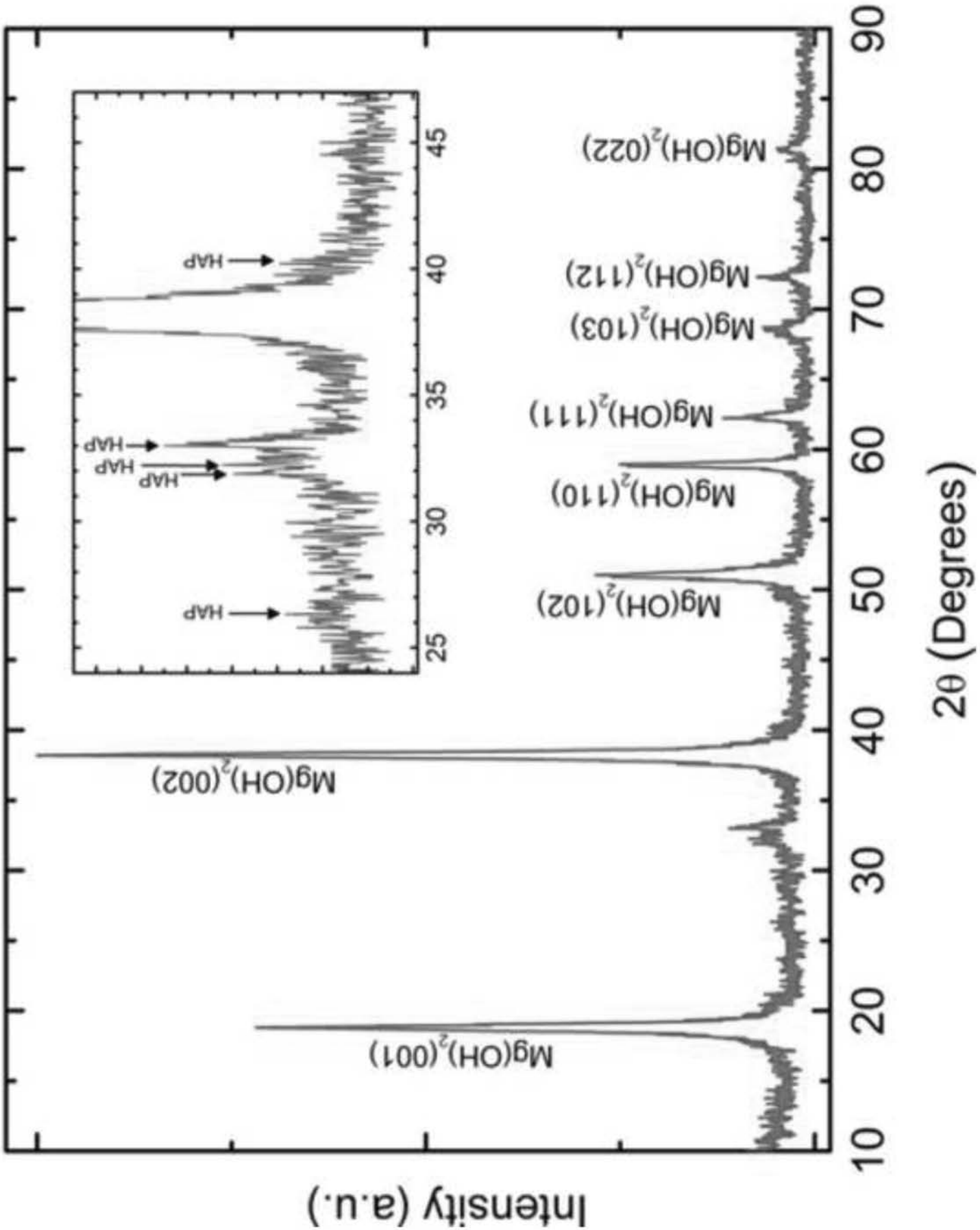

Figure11

Graphical Abstract (for review)